ELSEVIER

Remote Sensing of Environment

A Biogeophysical Approach for Automated SWIR Unmixing of Soils and Vegetation

Gregory P. Asner and David B. Lobell†*

Arid and semiarid ecosystems endure strong spatial and temporal variation of climate and land use that results in uniquely dynamic vegetation phenology, cover, and leaf area characteristics. Previous remote sensing efforts have not fully captured the spatial heterogeneity of vegetation properties required for functional analyses of these ecosystems, or have done so only with manually intensive algorithms of spectral mixture analysis that have limited operational use. These limitations motivated the development of an automated spectral unmixing approach based on a comprehensive analysis of vegetation and soil spectral variability resulting from biogeophysical variation in arid and semiarid regions. A field spectroscopic database of bare soils, green canopies, and litter canopies was compiled for 17 arid and semiarid sites in North and South America, representing a wide array of plant growth forms and species, vegetation conditions, and soil mineralogical-hydrological properties. Spectral reflectance of dominant cover types (green vegetation, litter, and bare soil) varied widely within and between sites, but the reflectance derivatives in the shortwave-infrared (SWIR2: 2,100–2,400 nm) were similar within and separable between each cover type. Using this result, an automated SWIR2 spectral unmixing algorithm was developed that includes a Monte Carlo approach for estimating errors in derived subpixel cover fractions resulting from endmember variability. The algorithm was applied to SWIR2 spectral data collected by the Airborne Visible and Infrared Imaging Spectrometer instrument over the Sevilleta and Jornada Long-Term Ecological Research sites. Subsequent comparisons to field data and geographical information system (GIS) maps were deemed successful. The SWIR2 region of the reflected solar spectrum provides a robust means to estimate the extent of bare soil and vegetation covers in arid and semiarid regions. The computationally efficient method developed here could be extended globally using SWIR2 spectrometer data to be collected from platforms such as the NASA Earth Observing-1 satellite. ©*Elsevier Science Inc., 2000*

INTRODUCTION

Dynamic climate and land use in arid and semiarid systems result in complex spatial and temporal variation of vegetation properties. Large-scale monitoring is critical for assessments of ecological change in these regions (UNEP, 1992). The tight coupling of vegetation cover to important hydrological and biogeochemical processes (e.g., Schlesinger et al., 1996; Schlesinger and Pilmanis, 1998) emphasizes the paramount importance of resolving vegetation and bare soil extent for functional analyses of these environments. However, the spatial extent of vegetation and bare soils is notoriously difficult to measure in arid and semiarid ecosystems using satellite imagery because variation occurs on the scale of a few meters or less.

Traditional multispectral classification approaches (e.g., using Landsat TM or NOAA Advanced Very High Resolution Radiometer (AVHRR)) have provided broad-scale estimates of vegetation greenness needed to link climate variability to ecological variation in arid and semiarid regions (e.g., Tucker et al., 1991; Myneni et al., 1996). However, past efforts have not provided the detailed biogeophysical information needed to monitor and model important changes in vegetation properties that can occur on the spatial scales of land use and biogeochemical cycling. For instance, a 30-m Landsat TM image can indicate spatial and temporal variation in green-

* Department of Geological Sciences and Environmental Studies Program, University of Colorado, Boulder

† Department of Applied Mathematics, Brown University, Providence

Address correspondence to Gregory P. Asner, University of Colorado, Department of Geological Sciences, Benson Building, Campus Box 399, Boulder, CO 80209-0399. E-mail: gregory.asner@colorado.edu

Received 20 September 1999; revised 2 December 1999.

REMOTE SENS. ENVIRON. 74:99–112 (2000)

655 Avenue of the Americas, New York, NY 10010

0034-4257/00/$–see front matter
PII S0034-4257(00)00126-7

ness (via the normalized difference vegetation index (NDVI)), but greenness estimates cannot easily separate the effects of changing vegetation condition (such as leaf area index) relative to vegetation cover (Carlson and Ripley, 1997). However, the difference is important from biogeochemical, hydrological, and land-use management points of view (Asner et al., 1998a; Wessman and Asner, 1998). Similarly, few multispectral classification approaches have quantitatively resolved the extent of senescent plant canopies (standing litter) and bare soil. Several efforts have focused on removing the effects of these constituents from greenness indices (e.g., van Leeuwen and Huete, 1996), but specific quantification of litter canopy and bare soil cover has proven elusive using existing multispectral approaches.

Imaging spectrometry provides near-contiguous, narrowband spectral analysis of the land surface that has proven useful for studying a wide variety of biophysical and geological processes (Green et al., 1998). One of the most common uses of imaging spectrometry is spectral mixture analysis, which capitalizes on unique spectral features of surface properties to estimate the subpixel cover fraction of specific land-surface types (Smith et al., 1994; Wessman et al., 1997). A central assumption is that land-cover endmembers sum linearly, or that departures from this assumption can be accommodated via residual cover fraction estimates or through the use of spectral endmember bundles (Bateson et al., 2000). Spectral mixture analysis has proven useful for studying various geological properties of arid and semiarid regions due to the distinct spectral signatures of constituent rock and soil minerals (Goetz et al., 1985). An important aspect of this approach is that the spectral properties of minerals are very consistent, allowing mixture modeling approaches to readily employ library endmembers (Clark, 1999).

In comparison to minerals, the spectral properties of live and senescent plant canopies are much less consistent. Variation in the condition, amount, and architectural orientation of plant tissues create canopy-level spectral variation that cannot be easily predetermined in a spectral library. It is this variation that motivates much of the biophysical remote sensing community, whose goals include monitoring the dynamics of vegetation phenology, greenness, leaf area, and energy absorption (e.g., Field et al., 1995; Myneni et al., 1997; Running et al., 1994; and many others). While the condition, amount, and architectural placement of the tissues can all contribute to variability in canopy reflectance, in reality, a subset of variables tend to dominate the variation within any given ecosystem or landscape (Asner, 1998). In arid and semiarid ecosystems, the amount of green and senescent foliage accounts for most of the spatial and temporal variation in canopy-level reflectance and energy absorption (van Leeuwen et al., 1997; Asner et al., 1998b). In addition, surface moisture and roughness strongly affect the soil reflectance (Jacquemoud et al., 1992; Pinty et al., 1998). Thus, vegetation and soil spectral endmembers collected in the field are difficult to apply in spectral mixture analyses at the spatial scales needed for regional monitoring efforts.

Several spectral unmixing approaches have been developed to address variation in vegetation and soil endmember spectra (e.g., Bateson et al., 2000; Smith et al., 1994). The most flexible approaches derive ranges of spectral endmembers from field data or image pixels and then incorporate this variability into subpixel cover estimates (e.g., Bateson et al., 1999). Efforts to incorporate endmember variability (e.g., via fuzzy endmember sets or bundles) are physically consistent with the natural variability that occurs among vegetation and soil spectra, but broad variation in endmembers often leads to wide ranges of plausible cover fraction results. Therefore, it is desirable to establish features of the spectrum that, for the most common land-cover types, display the least spectral variability while remaining distinct from one another.

Previous work involving arid and semiarid vegetation in North and South America indicated high spectral variability of live and senescent canopies (Asner, 1998; Asner et al., 2000). Most of this variation was attributed to the spatial and temporal heterogeneity of leaf and litter area index (LAI, LitterAI). Similarly, it was observed that soil reflectance varied within and between sites due primarily to moisture content. However, among the sites visited in those studies, there were consistent spectral derivatives for green vegetation, litter, and bare soils in the shortwave-infrared region between 2,100 nm and 2,400 nm (the "SWIR2" region). Although the overall reflectance of each cover type varied sharply within and across sites and the spectral derivatives varied throughout most of the visible and NIR (NIR), the SWIR2 spectral derivatives varied little and were distinct between land-cover types (Fig. 1).

The consistency of the SWIR2 derivative spectra of green vegetation canopies results from foliar water acting as a very strong absorber of SWIR2 radiation (Wooley, 1971; Ustin et al., 1999). At LAI values of 1.0, the SWIR2 region nearly saturates at the reflectance values typical of green vegetation, and the SWIR2 derivative spectra are consistent at LAI of 1.0 and greater (Asner, 1998). The distinct features in SWIR2 litter reflectance result from stretching, bending, and overtones of C-H and O-H bonds associated with organic carbon compounds interacting with shortwave radiation (Curran, 1989). Soil spectra collected by Asner (1998) had a distinctive absorption feature centered near 2,200 nm, which results from combinations and overtones of hydroxyl absorption in the clay lattice structure of soils that dominate many arid and semiarid environments (Ben-Dor et al., 1999). Although the SWIR2 soil spectra varied with mineralogy and clay content (cf., Drake et al., 1999), this variation was limited to a much smaller range

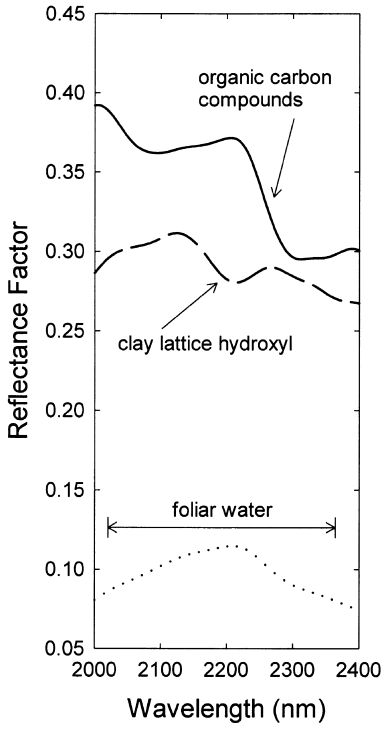

Figure 1. Typical spectra of green canopy (dotted), litter (solid), and bare soil (dashed) in SWIR2 region (2,000–2,400 nm). Primary causes of major spectral features are provided.

of values in the spectral derivatives. While the overall reflectance of both litter canopies and bare soils varied sharply from place to place, their SWIR2 derivative spectra were consistent and distinct.

Based on these earlier observations, we sought to capitalize on the apparent consistency of the SWIR2 derivatives by developing a spectral unmixing algorithm to estimate vegetation and bare soil extent in arid and semiarid regions. Our approach was based on a three-component effort: (1) an expanded spectral survey of green vegetation, standing and surface litter, and bare soils at 17 representative sites in North and South America; (2) establishment of a reliable set of SWIR2 spectral signatures for each dominant land-cover types found in arid and semiarid regions; and (3) development of a fast, automated spectral unmixing approach that includes statistical estimation of uncertainty in the derived subpixel cover fractions. This paper reports the results of each step and a further extension to a spectral index method for potential use with future multispectral imagers.

METHODS

Field Spectroscopy

To develop a broadly applicable spectral unmixing approach for arid and semiarid ecosystems, our strategy was first to quantify the biogeophysical variability of the dominant endmembers at as many field sites and under as many conditions as we thought necessary to ultimately acquire statistical confidence in the subpixel cover fractions. Recognizing the multitude of highly variable green and senescent plant canopies and bare soil in these regions, we felt that a thorough survey of their spectral properties would yield the most generalizable endmember data set needed to establish the most predictable spectral region for mixture modeling. The field spectral survey included vegetation types from grasslands, shrublands, woodlands, and savannas in desert, semidesert, temperate, subtropical, and tropical climates (Table 1). The data set included green and litter canopies of more than 450 herbaceous and woody plant species, representing a wide array of growth forms, physiologies, canopy architectures, intracanopy shading, tissue chemistries, and tissue optical properties (Asner, 1998; Asner et al., 2000; and unpublished data). LAI ranged from 0.2 to 7.9 among green canopies, while litter area index (litterAI) varied from 0.3 to 6.6 for senescent herbaceous canopies.

The data were collected using a full-range (350–2,500 nm) spectrometer with an 18° sensor foreoptic (Analytical Spectral Devices, Inc., Boulder, CO, USA). This instrument collects data in 1.4-nm intervals from 350–1,100 nm and 2.2-nm intervals in the remaining shortwave-infrared (1,100–2,500 nm). All measurements were collected within 1 hour of local solar noon on clear-sky days. The sensor was held 1.5 m above the top of each canopy or soil surface in the nadir position. A ladder was used to obtain spectra of large shrubs and trees at some of the sites. Radiance measurements were converted to reflectance using a Spectralon (Labsphere, Inc., Stratton, NH, USA) calibration panel, which was measured immediately before each canopy or soil measurement.

The 98,423-spectrum database was analyzed to find which wavelength region was most consistent for use in a generalized spectral unmixing model. Endmember bundles were then constructed to represent the variability in the selected wavelength region. Final preparation of the endmember sets included high-frequency filtering and linear transformation to emphasize spectral shape. Two possibilities were considered for characterizing spectral shapes: derivative spectra and "tied" spectra, with the latter defined as subtracting the value at one wavelength (the tie point) from all other wavelengths. As will be demonstrated, the tied spectra can be advantageous because they are less sensitive to very narrowband noise that can arise in derivative data.

Spectral Mixture Analysis

Most spectral mixture models represent the reflectance of an image pixel as the linear combination of endmember spectra [see Eq. (1)]:

Table 1. Description of Field Sites Visited to Collect Canopy and Bare Soil Endmember Spetra

Ecosystem/Vegetation Type	*Site Location*	*Resource Area*	*Annual Precipitation*[a]	*Dominant Soil Type*	*Canopy-Level LAI Range*[b]	*Spectral Data Collected*[c,d]
Desert grassland	Jornada LTER	Chihuahuan Desert	230	Aridisols	0.1–0.8	G_L (680) B (142)
Desert scrub/shrubland	Jornada LTER, NM	Chihuahuan Desert	230	Aridisols	0.9–3.1	S (452) B (1105)
Arid grassland	Sevilleta LTER, NM	Great Plains, Great Basin Shrub-Steppe	255	Entisols	0.2–1.6	G_G (79) G_L (394) B (91)
Desert shrubland, shrub-steppe	Sevilleta LTER, NM	Great Plains, Great Basin Shrub-Steppe	255	Entisols	0.8–3.9	S (178) B (1,340)
Desert scrub/shrubland	Tucson, AZ	Sonora Desert	290	Aridisols	0.6–4.4	S (262) B (1,003)
Semiarid shortgrass Prairie	Colorado Springs, CO	Rollings Plains	385	Alfisols/Mollisols	0.4–1.7	G_G (167) G_L (605) B (202)
Semiarid woodland	Colorado Springs, CO	Front Range Woodland-Grassland Transition	402	Entisols	0.6–4.4	S (158) B (790)
Semiarid/temperate tallgrass prairie	Boulder, CO	Rolling Plains	485	Alfisols	0.5–3.6	G_G (1,310) G_L (480)
Semiarid shrubland/ woodland	Sonora, TX	Edwards plateau	575	Alfisols/Entisols	0.6–4.9	S (38) B (56)
Xeromorphic woodland	San Carlos, CA	Mediterranean Chaparral	605	Entisols	1.1–5.6	S (45) B (192)
Annual grassland	San Carlos, CA	Coastal Hills	611	Entisols	0.6–3.7	G_G (5,071) G_L (7,990) B (32)
Temperate tallgrass prairie	Vernon, TX	Rolling Plains	640	Mollisols/ Entisols	0.3–4.2	G_G (4,203) G_L (3,764) B (230)
Temperate savanna	Vernon, TX	Rolling Plains	640	Mollisols/ Entisols	0.9–5.1	S (691) G_G (7,659) G_L (4,760) B (10,050)
Subtropical savanna	Alice, TX	Rio Grande Plains	720	Alfisols/Ultisols	0.7–5.4	S (76) G_G (123) G_L (2,210) B (535)
Tropical savanna	Brasilia, Brazil	Cerrado	1490	Ultisols/Oxisols	0.4–3.2	S (61) G_G (6,440) G_L (9,780) B (5,051)
Tropical woodland	Brasilia, Brazil	Cerradao	1490	Ultisols/Oxisols	0.7–4.8	S (26) B (884)
Tropical grassland	Brasilia, Brazil	Campo Limpo/ Campo Sujo	1490	Oxisols/Ultisols	0.6–6.9	G_G (7,650) G_L (10,058)

Cover types and number of spectra are listed in far right column.
[a] Measured using Licor LAI-2000 Instrument (e.g., Asner et al. 1998b).
[b] Values in mm.
[c] S=green shrub or tree canopy, G_G=green herbaceous canopy, G_L=senescent herbaceous canopy (litter), B=bare soil.
[d] Values in parentheses indicate number of spectra collected.

$$\rho_{pixel}=\sigma[\rho_e \cdot C_e]+\varepsilon=[\rho_{veg} \cdot C_{veg}+\rho_{soil} \cdot +\rho_{litter} \cdot C_{litter}]+\varepsilon \quad (1)$$

where ρ and C are the reflectance and cover fraction of each endmember, respectively, and ε is an error term. An additional endmember is often included in these algorithms to account for the contribution of intra- and intercanopy shadow. However, this fraction is difficult to isolate in the field or in image pixels; thus, it is often used as a residual endmember. Our field experience indicated that shadow can be taken into account if the spectral database includes canopies and small areas with mixed sunlit and shaded surfaces. We also recognized that shade causes the overall reflectance of the underlying material to decrease but does not sharply alter the shape (derivatives) of the SWIR spectra. By assuming that the effects of shade on the reflectance of vegetation and soil surfaces are independent of their scale, field spectra that include a sufficiently heterogeneous mix of sunlit and shaded surfaces can account for the presence

of shade at the pixel level. Both radiative transfer (for intracanopy shade) and geometric-optical (for intercanopy shade) theories and experiments have shown this to be a reasonable assumption (Caulfield et al., 1992; Myneni et al., 1989; Ross, 1981).

In an effort to incorporate both spectral endmember variability and uncertainty in the unmixing approach, we devised a probabilistic method using endmember sets that embodied the range of variation present in the field. A Monte Carlo unmixing (MCU) strategy was developed to derive subpixel cover fractions with statistical confidence intervals. The MCU approach involves generating a large number of endmember (green vegetation, litter, and soil) combinations for each pixel (n=50–200 or more) by randomly selecting spectra from the database of field spectra. The performance was evaluated using raw reflectance, derivative, and tied endmember spectra. Based on a series of preliminary tests of the model, the cover fractions resulting from the MCU procedure invariably had a normal distribution for each pixel. We therefore used the mean values to estimate the fractional cover of each endmember and the standard deviation to form a confidence interval for the true fraction. As a result, this approach allowed for a quantitative measure of how well the cover estimates were constrained using the reflectance, derivative, and tied spectral endmembers from an entirely general endmember database and in any wavelength interval.

Evaluation Using AVIRIS Imagery

The MCU approach was evaluated using Airborne Visible and Infrared Imaging Spectrometer (AVIRIS) data collected over two arid grassland-shrubland regions in New Mexico. The Jornada and Sevilleta Long-Term Ecological Research (LTER) sites are located near Las Cruces and Socorro, NM, respectively. Each site contains spatially complex gradients of grassland, mixed grass-shrubland, and shrubland ecosystems (see www.lternet.edu). The AVIRIS data were collected in May 1997 when most of the grasslands canopies were senescent, while the shrub canopies were predominantly green. Bare soil is ubiquitous throughout both sites, but varied in spatial extent from 1% to 50% in some grassland areas to 40% to 95% in various shrubland sites (Schlesinger et al., 1996; White et al., 2000; Asner et al., 2000). Other characteristics of the Jornada and Sevilleta LTER sites are provided in Table 1.

The AVIRIS instrument collected upwelling radiance data in 224 optical channels [~10-nm bandwidth at full width half maxima (FWHM)] covering the 380-nm to 2,500-nm region. The AVIRIS was carried onboard the NASA ER-2 aircraft, which flew at 20-km altitude during image acquisition, creating approximately 20-m pixels. Radiance data were converted to apparent surface reflectance using the ATREM atmospheric code (Gao et al., 1993), which employs the 6S scattering code for atmospheric gases and aerosols (Vermote et al., 1997). The atmospherically corrected AVIRIS data were compared to field spectrometer data collected at a large dry riverbed area near Sevilleta and a bare soil parking lot at Jornada. The AVIRIS and field spectrometer data were found to be statistically similar, indicating good accounting of atmospheric constituents, such as aerosol and water vapor, in the AVIRIS correction.

During the time of AVIRIS overflight, field spectrometric data were collected for each major land-cover type found at Jornada and Sevilleta LTER sites (Table 1). In addition, canopy and landscape structural properties were assessed using a variety of instruments and techniques. Details of the measurements and methods were provided by White et al. (2000) and Asner et al. (2000), but they included: (1) LAI using both direct and indirect measurement methods; (2) vegetation cover fraction using transect surveys, quadrat analysis, digital camera, air photos, and airborne laser altimetry techniques; (3) plant tissue optical properties using a spectrometer and integrating sphere; (4) canopy architectural properties; (5) plant height and width; and (6) species composition surveys. A subset of these measurements were used to evaluate the sensitivity of the MCU procedure to both canopy and landscape characteristics. In addition, Sevilleta LTER personnel regularly collect detailed vegetation, litter, and bare soil cover data along 1,600-m transects from five diverse grassland and shrubland ecosystems (see http://sevilleta.unm.edu/). Sevilleta cover data collected in May 1997, very near in time to the AVIRIS overflight, were used in addition to our own data to evaluate the MCU approach.

RESULTS AND DISCUSSION

Monte Carlo Unmixing Approach

The spectral properties of green canopies, standing and surface litter, and bare soils measured at the sites listed in Table 1 were statistically similar to the subset of spectra collected by Asner (1998). Moreover, for each surface type, the spectral variability at any given site was usually equal to that of the entire data set (t-tests by wavelength, $p<0.05$). Green canopy reflectance varied the most in the NIR between 700 nm and 1,300 nm and the least in the SWIR2 region (Fig. 2). Both litter canopy and bare soil reflectance were most variable in the SWIR (1,300–2,500 nm); however, upon converting the data to spectral derivatives (approximated as finite differences), the most consistent spectral region was the SWIR. Green canopy spectral derivatives were also very consistent in this wavelength region. The consistency of the SWIR derivatives for each cover type indicated the strong potential for using this spectral region in a mixture decomposition of arid and semiarid environments.

Of equal importance to the consistency of endmembers in a spectral unmixing method is the separability of

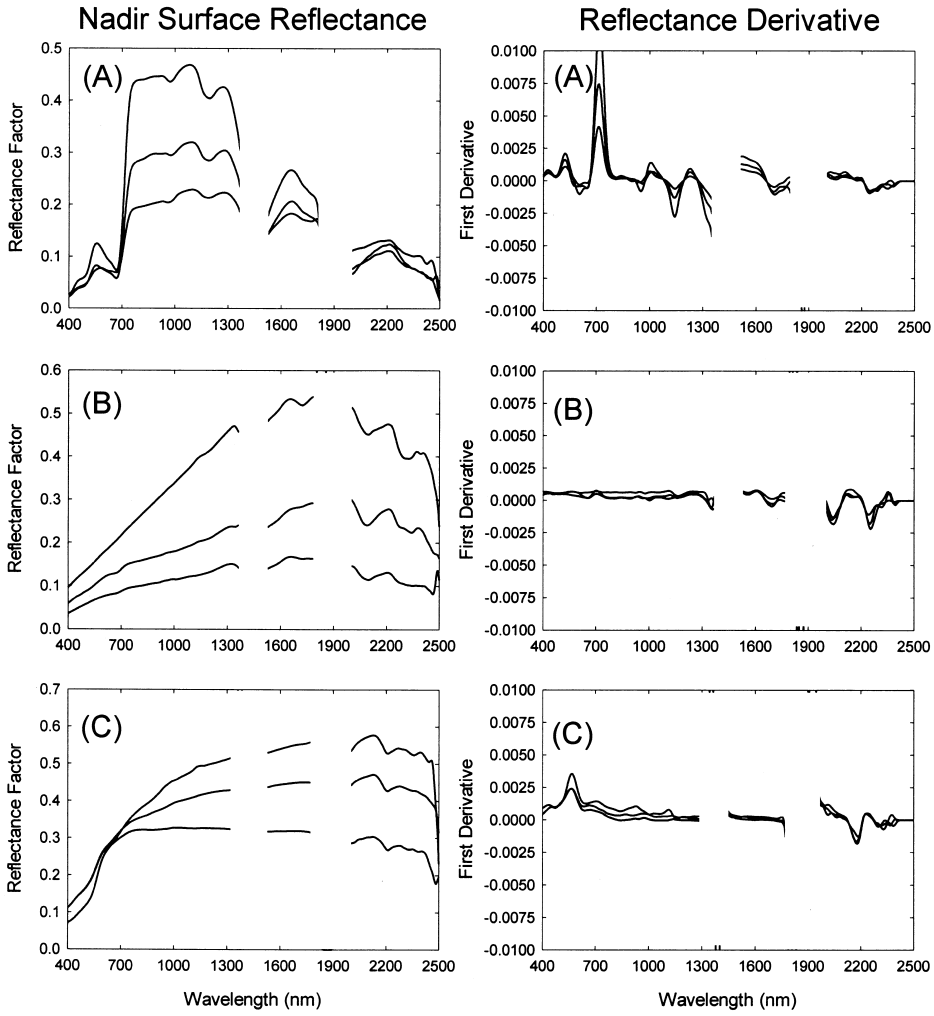

Figure 2. Sample nadir reflectance and derivative spectra (400–2,500 nm) of (A) green and (B) senescent (litter) canopies and (C) bare soils collected at 17 arid and semiarid sites in North and South America. Full range of variability is shown.

those endmembers. The distinctness of each endmember largely determines the success or failure of the spectral unmixing approach. Of the possible spectral regions, the SWIR2 remained the best option for unmixing using derivative spectra. Green canopy, litter, and bare soil covers were distinct in the SWIR2 due to the features described in Fig. 1. In other spectral regions, two of the dominant cover types often showed distinct and readily separable features, but only in the SWIR2 were all three endmembers consistently distinct (Fig. 2). For example, the visible-NIR region provided good separation of green canopies from litter or bare soils, but differences between litter and bare soil were exceedingly difficult to detect in this part of the spectrum (also found by van Leeuwen and Huete, 1996; Asner, 1998; Asner et al., 2000).

Overall, the SWIR2 spectral region provided the most consistent and distinct endmembers (as derivatives). Of over 98,000 spectra collected, there was one major exception to this finding. Black grama (*Boutelua eriopoda*) is a common forage grass found in arid ecosystems of the Southwest United States (USDA, 1934). While its green canopy spectra were similar to those of other herbaceous species, its senescent canopy spectra were distinct from other standing litter canopies. Black grama turns to a brown-black color during senescence, resulting in both lower reflectance throughout the shortwave spectrum and a flattened (small derivatives) SWIR2 spectral region. For this reason, the derivative spectra of senescent black grama can look similar to that of green vegetation in the SWIR2, and a SWIR2 spectral unmixing algorithm will tend to place the areas covered by black grama litter into the "green canopy" results. As explained later, we devised a separate approach for delineating senescent black grama from green canopy cover to remedy this problem.

Despite this exception, the SWIR2 remained the best choice for separating green canopies, standing and surface litter, and bare soils in the arid and semiarid environments visited during the field survey (Table 1). Based on these results, we tested the MCU procedure for estimating the fractional abundance of these cover types in simulated SWIR2 data. The mean green canopy and litter and soil spectra collected in the field were convolved to AVIRIS spectral channels and then used in a

Table 2. Effect of Noise on Calculated Cover Fractions Using Tied and Derivative Spectra

Modeled Fractions	Noise level (%)	Litter Fraction		Leaf Fraction		Soil Fraction	
		Tied	Derivative	Tied	Derivative	Tied	Derivative
(a)							
Litter=0.333	0	0.34	0.34	0.33	0.33	0.34	0.34
Green canopy=0.333	5	0.34	0.33	0.33	0.34	0.34	0.34
Soil=0.333	10	0.33	0.34	0.33	0.32	0.34	0.34
	15	0.32	0.24	0.33	0.42	0.35	0.34
(b)							
Litter=0.8	0	0.82	0.81	0.08	0.10	0.10	0.09
Green canopy=0.1	5	0.81	0.79	0.09	0.12	0.10	0.09
Soil=0.1	10	0.80	0.80	0.09	0.11	0.10	0.09
	15	0.78	0.63	0.11	0.28	0.11	0.09
(c)							
Litter=0.1	0	0.11	0.12	0.80	0.77	0.09	0.11
Green canopy=0.8	5	0.11	0.11	0.80	0.78	0.10	0.11
Soil=0.1	10	0.11	0.11	0.80	0.78	0.10	0.11
	15	0.11	0.08	0.80	0.81	0.09	0.10
(d)							
Litter=0.1	0	0.09	0.08	0.10	0.11	0.82	0.81
Green canopy=0.1	5	0.09	0.08	0.10	0.11	0.82	0.81
Soil=0.8	10	0.08	0.09	0.10	0.08	0.83	0.83
	15	0.07	0.01	0.10	0.16	0.84	0.83

Four different spectral mixing scenarios were tested. Specified noise level signifies the standard deviation of normally distributed noise as a percent of the modeled spectra at each wavelength.

sensitivity analysis. We first investigated the effects of varying noise levels on the MCU-derived fractions using both derivative and tied spectra. Normally distributed noise with a mean of zero and a standard deviation ranging from 0% to 15% of the signal was added to each of four modeled spectra (each of which was a different combination of the three mean endmember spectra; Table 2). The noise represented errors that could arise from sources such as insufficient signal-to-noise detector, inaccurate atmospheric removal, and the presence of unaccounted cover types. The MCU procedure was then performed on each simulated spectrum using 100 endmember-database runs in the 2,078-nm to 2,278-nm wavelength interval.

In the baseline case (0% noise), both the tied and derivative methods yielded accurate fractions for each of the four modeled spectra (Table 2). However, the tied spectra were much less susceptible to noise in comparison to the derivative spectra. For example, in the case where the modeled spectra contained 80% litter, the litter fraction calculated using derivative spectra was 63% (at 15% noise level), while the fraction from the tied spectra was 78%. The results using the tied spectra were more reliable because they emphasize the broad shape of the spectra, while the derivative spectra concentrate on local differences and are thus more vulnerable to high-frequency noise. Overall, the method displayed outstanding performance even at 15% noise level, which we

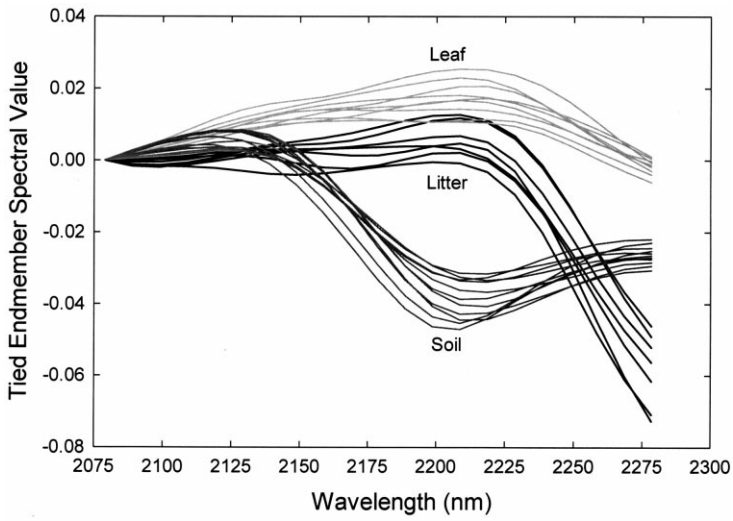

Figure 3. Examples of SWIR2 tied endmember spectra, showing full range of variability within endmember classes.

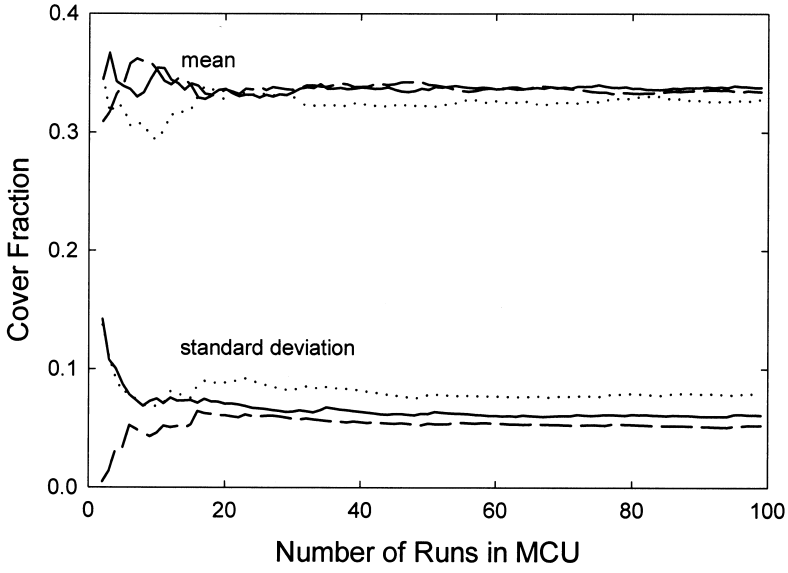

Figure 4. Mean and standard deviation of green canopy (dotted), litter (solid), and bare soil (dashed) fractions versus number of runs in the MCU algorithm.

considered to be very high and unlikely. Therefore, the tied SWIR2 spectra were adopted for use in all subsequent unmixing applications (Fig. 3).

The MCU approach was used to propagate uncertainty in endmember spectra to the final subpixel cover fraction results. Monte Carlo methods are popular due to their simplicity and interpretability, but they can be cumbersome if too many iterations are required to develop confident statistics. Thus, an important factor to consider was the minimum number of inversions, or runs, in the MCU needed to converge to a given mean and standard deviation. Figure 4 shows the calculated means and standard deviations from MCU performed with a varying number of runs on a spectrum modeled from equal fractions of each field endmember. The results showed that additional runs beyond 30 have little effect on the derived fractions. A conservative value of 50 runs was therefore chosen for the remainder of the study.

AVIRIS Imagery

The MCU technique was used with the tied SWIR2 spectra to estimate the fractional cover of green canopies, litter, and soil in the Jornada and Sevilleta AVIRIS scenes. At the Jornada site, the relatively small standard deviations (~5%) of the cover fraction values indicated that the SWIR2 region provided the spectral endmember consistency and distinctiveness needed to estimate the

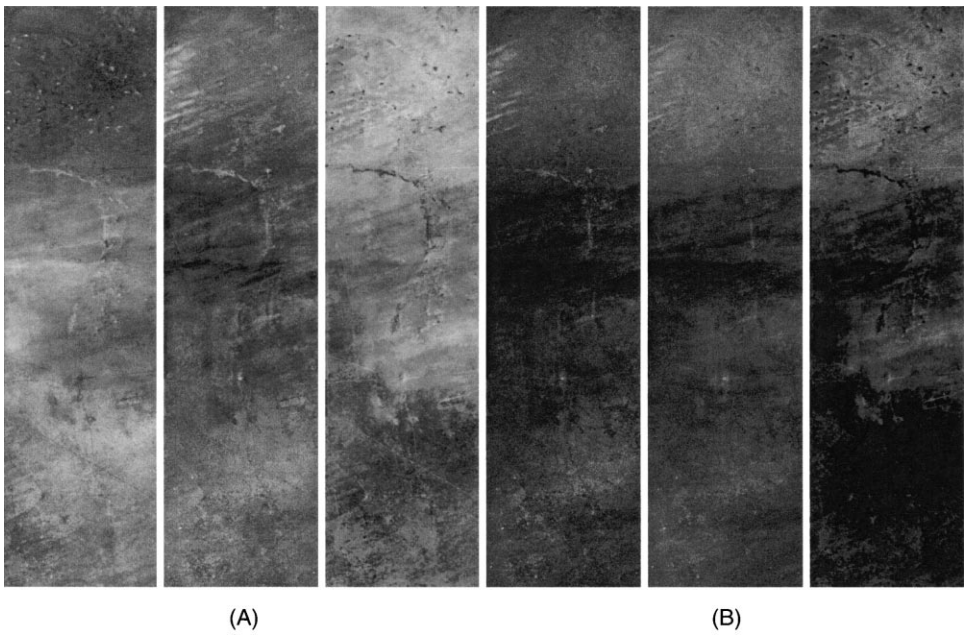

Figure 5. Cover fraction images derived from SWIR2 MCU of AVIRIS data collected over Jornada LTER site. (A) Mean cover fraction images from MCU of green canopy, litter, and bare soil are shown (left to right). (B) Standard derivation images of cover fractions.

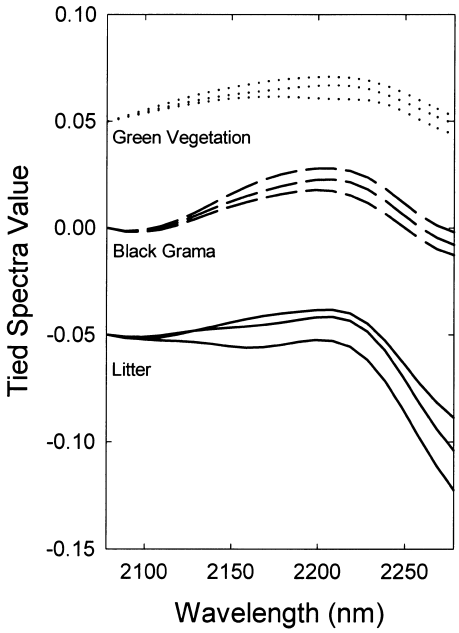

Figure 6. SWIR2 tied endmember spectra of black grama in comparison to endmember spectra of green canopy and litter. Spectra are offset by 0.05 for clarity.

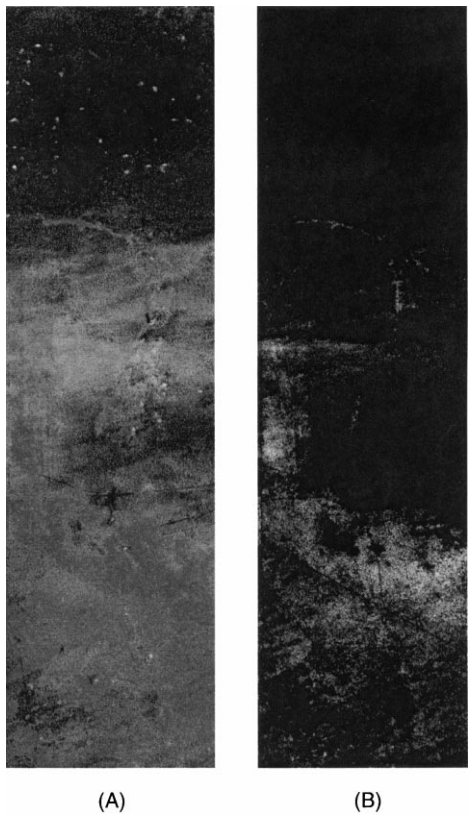

Figure 7. True green canopy (A) and black grama (B) cover fractions for Jornada AVIRIS scene, derived from fractions in Fig. 5 and red-edge MCU.

subpixel cover fractions with statistical confidence (Fig. 5). Had the endmembers been less consistent or distinct from one another, the Monte Carlo technique would have produced much larger standard deviation images. We tested a variety of other spectral regions, such as the visible and NIR, but none resulted in the narrowness and accuracy (compared to field data) of resultant endmembers as was found when using the SWIR2 region.

As expected, the green canopy fraction was overestimated in some areas of Jornada and Sevilleta because the tied spectra of black grama litter look similar to those of green canopies in the SWIR2 region (Fig. 6). To account for this situation, a second wavelength interval was used to partition the green canopy fraction into black grama litter and true green canopy. An ideal location for this separation is the "red-edge," where green vegetation has a very consistent and steep slope, while soil and litter spectra are relatively flat (Hall et al., 1990). A second-stage Monte Carlo unmixing was performed in a 20-nm (692–712 nm) section of the red-edge, while the bare soil and litter fractions derived from the original SWIR2 unmixing were used to constrain the inversion. The red-edge was not simply added to the SWIR2 for a single unmixing. We found that soil and litter spectral variability in the red-edge was far greater than in the SWIR2, which would have led to erroneous estimates of all endmembers had a single unmixing been performed. The second-stage unmixing was thus used to isolate black grama as an optional second step, necessary only in areas where it is likely to be a major scene component.

The second-stage MCU correctly predicted the spatial extent of black grama grasslands that otherwise would have been lumped into the "green canopy" cover fraction (Fig. 7). For many applications, separation of black grama from true green canopy may not be needed, such as in monitoring the broad rates of desertification, which is known to be occurring in these regions and others worldwide (Schlesinger et al., 1990; UNEP, 1992). Desertification tends to increase the bare soil extent, so this first level of monitoring is satisfied by the single-stage MCU approach presented here. For analyses of climate and land-use effects on vegetation phenology, diversity, abundance, and condition, the second-stage MCU is required to separate functionally diverse vegetation types, such as senescent black grama and actual green canopies, which denoted shrubland cover in these particular AVIRIS scenes. It is also highly useful for rangeland ecology and management efforts (NMAES, 1970).

The final resultant Jornada and Sevilleta regional fractions were consistent with available GIS and vegetation maps derived from field surveys and air photos (Figs. 8 and 9). For example, the Jornada results agreed with a vegetation map recently completed by LTER site personnel (Fig. 8; map courtesy of B. Nolen). Green can-

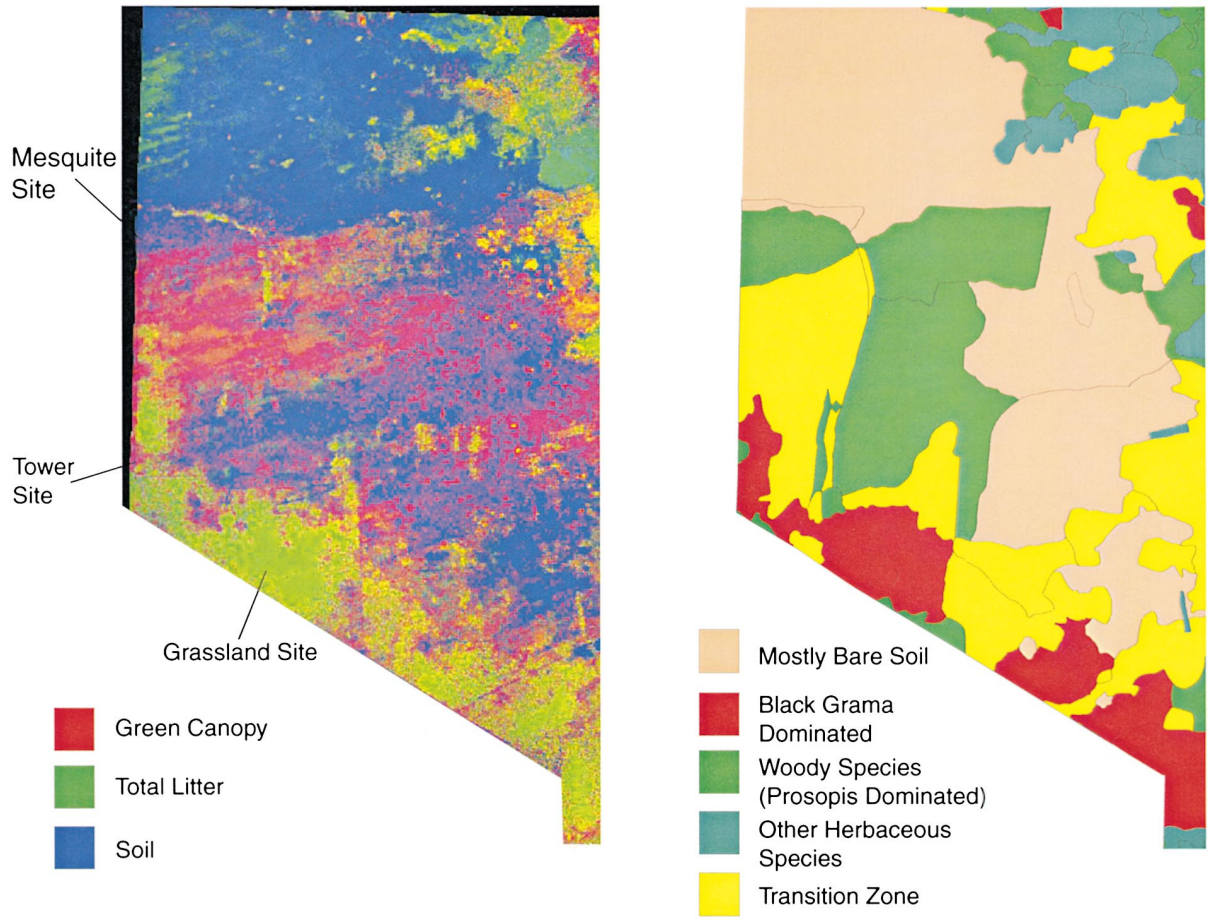

Figure 8. Color composite of true green canopy, total litter, and bare soil fractions in comparison to a field-based vegetation map for Jornada LTER site. Locations and names of field sites are also shown. Map courtesy of B. Nolen.

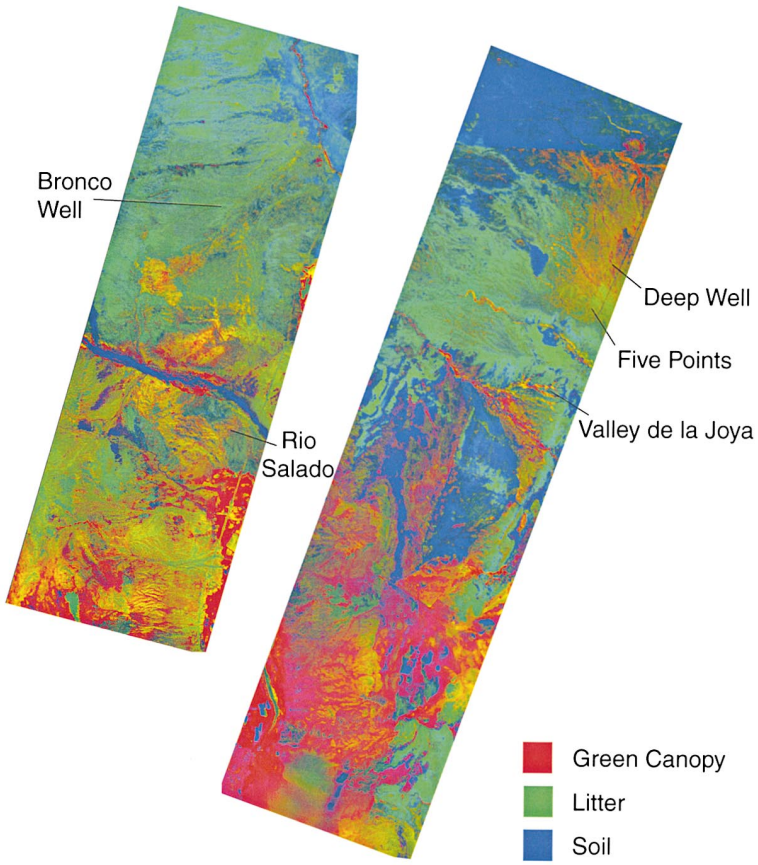

Figure 9. Color composite of true green canopy, total litter, and bare soil fractions derived from MCU for nine geo-referenced AVIRIS scenes from Sevilleta LTER site. Location and names of field sites are also shown.

opy cover fractions corresponded spatially with woody species, such as *Prosopis glandulosa* (mesquite), which were green during the AVIRIS overflight in May 1997. Litter cover fractions were consistent with grassland areas dominated by *Boutelua eriopoda* (black grama), which was highly senescent at that time. Similar comparisons of the Sevilleta results (Fig. 9) showed consistency with existing vegetation maps derived from aerial photographs and field surveys (map comparison not shown). These results also emphasized the strategic utility of acquiring imaging spectrometer data of these ecosystems in the late spring season when functionally unique vegetation types (woody and herbaceous communities) are in different phenological stages and are thus spectrally separable.

Comparison of the MCU and field-derived bare soil and vegetation fractions showed a high degree of accuracy at the site level (Fig. 10). In this study, green plus senescent vegetation cover was not well correlated with the plant area index (=LAI+LitterAI) of the individual canopies (Fig. 11). These results indicated that the SWIR2 region and MCU approach were primarily sensitive to the horizontal extent of vegetation types, and not to the vertical density (LAI) of the individual canopies present within pixels. Isolation of the vegetation and bare soil cover fractions within image pixels is needed for hydrological and biogeochemical analyses in arid and semiarid regions (Asner et al., 1998a; Asner et al., 1998b; Schlesinger and Pilmanis, 1998). It also provides a means to monitor changes in vegetation cover associated with land-use and climate impacts such as desertification (UNEP, 1992).

We contend that the SWIR2 Monte Carlo unmixing method is robust for two reasons. First, the method provides a means to directly incorporate endmember variability into the spectral unmixing effort. Analogous methods have been used to account for endmember variability (e.g., Bateson et al., 2000), so this development is not fully unique. However, in combination with the establishment of SWIR2 tied spectra, whose selection was based on the stability of the spectral endmembers in a biogeophysically diverse field survey, our approach is both physically robust and computationally efficient, lending itself to complete automation. Our method provided verifiably accurate results without ground calibration or excessive image preparation. While we think that the approach is especially robust in arid and semiarid vegetation and soil types, we also have strong evidence suggesting its utility in other scenarios, such as forested ecosystems (Asner, unpublished data).

Derivation of a Three-Channel Multispectral Approach

The observation that soil, litter, and green canopy spectra possess consistent shapes in the SWIR2 is the key to our probabilistic spectral unmixing method. The small variability within each endmember class suggests that representative spectra (e.g., the average from each endmember set) can be used for quick fraction estimation. This results in a fixed endmember matrix that can be conveniently transformed into an index through inversion of the singular value decomposition (SVD) of the endmember matrix. We employed this strategy to test the possibility of using a small number of wavelengths that might best characterize the different spectra. The goal was to determine if a simple multispectral SWIR2 approach could yield results that are as accurate as those derived using continuous SWIR2 spectral signatures. A major consideration in this analysis was the width of the band passes, because broadening the bands can both increase the amount of signal received at the sensor and significantly lower the cost of hardware development. We explored the use of three bands with varying FWHM centered at 2,080 nm, 2,210 nm, and 2,270 nm. The first

Figure 10. Comparison of actual and predicted cover fractions from field sites at Jornada and Sevilleta LTER sites.

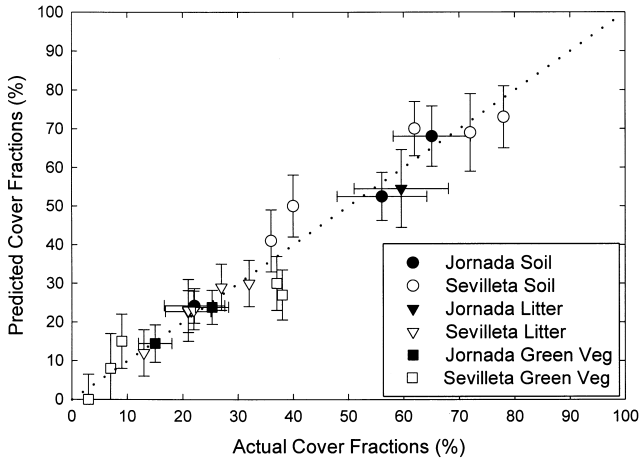

Figure 11. Comparison of predicted cover fraction and total plant area index (=leaf+litter area index) collected at Jornada and Sevilleta LTER sites.

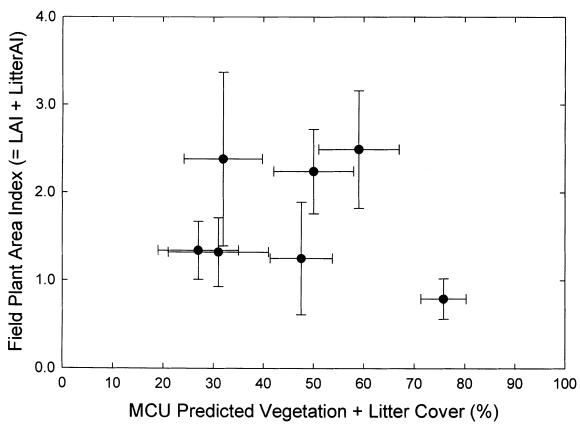

Table 3. Regression Coefficients and R^2 Values for Cover Fractions Derived from the Full 21-Channel Compared to a three-Channel Index in the Monte Carlo Unmixing of the Jornada LTER site, NM

Endmember	*Bandwidth (FWHM)*	*Slope*	*Offset*	R^2
(a) Litter	10 nm	1.004	−0.001	0.848
	20 nm	0.895	0.078	0.967
	30 nm	0.938	0.007	0.956
	40 nm	0.917	0.019	0.946
(b) Green canopy	10 nm	0.946	0.009	0.937
	20 nm	0.969	0.001	0.953
	30 nm	0.869	0.126	0.961
	40 nm	0.845	0.154	0.952
(c) Soil	10 nm	0.950	0.028	0.965
	20 nm	0.918	−0.006	0.986
	30 nm	0.900	−0.037	0.988
	40 nm	0.881	−0.057	0.989

The index consists of three bands centered at 2,080 nm, 2,210 nm, and 2,270 nm.

band was chosen as a reference or tie point; the second to distinguish soil from plant material; and the third to separate litter from green canopy (see Fig. 4). For each bandwidth, the endmember spectra were resampled to the given band positions and FWHM and then averaged to produce a mean endmember spectrum at the simulated resolution. The indices resulting from these average spectra were then applied to the entire Jornada AVIRIS scene, which was also resampled to the given wavelengths and FWHM.

Table 3 shows the regression coefficients between the fractions derived in this manner and the fractions derived from the full 21-channel SWIR2 unmixing. In general, the fractions derived from these simple indices were in agreement with the full MCU results. Moderate bandwidths (e.g., 20–30 nm) appeared to yield optimal results, since wider bandwidths tended to confuse litter and green canopy and narrow bandwidths were more influenced by high-frequency noise. Of particular interest was the stability of the soil fraction results which had an $R^2 > 0.95$ and offset $< 6\%$ at all bandwidths. We believe that these indices, derived directly from a spectral unmixing framework, suggest a promising avenue for physically consistent cover estimates from future multispectral sensors. However, we also emphasize that a three-band SWIR2 approach may not fully account for endmember variability, which could arise from pixel to pixel or site to site. Thus, we qualify the three-band results presented here and reserve future efforts to verify the stability of simpler multispectral index approaches such as this one. Nonetheless, these preliminary results are promising and may warrant an extension of Landsat-like instruments by replacing the typical single SWIR2 channel with three channels that are sensitive to vegetation and bare soil extent in arid and semiarid ecosystems.

CONCLUSIONS

We have developed and successfully tested an efficient probabilistic approach for quantifying the subpixel spatial extent of vegetation and soils in arid and semiarid ecosystems using spectral reflectance signatures from the shortwave-infrared region between 2,100 nm and 2,400 nm (the SWIR2 region). We believe the method provides accurate cover estimates independent of the factors that typically confound spectral unmixing algorithms utilizing full-optical range multispectral or hyperspectral reflectance signatures. These factors, such as soil moisture, leaf and litter area index, canopy architecture, and tissue optics, do not cause significant variation in the SWIR2 derivative or "tied" spectra. Thus, our approach benefits from the consistency with which the endmembers can be predicted. The variation that does exist is propagated throughout the method using a fast Monte Carlo approach. Methods that employ full-optical range spectra are prone to inaccuracies due to albedo and visible-NIR derivative variation, or they provide very wide ranges of fractional cover results when endmember variation is taken into account.

This approach represents more of a philosophy about how pixel-scale spectral signatures can be decomposed into vegetation and soil estimates than it does an algorithm for spectral unmixing. It represents a methodology that includes: (1) defining the spectral variability of major component endmembers across broad biogeophysical gradients; (2) seeking out the type of endmember signature (e.g., reflectance, derivative, tied in a given spectral region) that is most consistent as vegetation and soil properties, such as leaf angle, tissue optics, LAI, and soil moisture, vary spatially and temporally; and (3) allowing for the variability in the selected endmember spectra to propagate through to the final unmixing results. While no linear spectral unmixing approach will get the answer correct every time an image is processed, we feel that the MCU approach provides the physical consistency needed to develop reliable estimates of bare soil and total vegetation (live+litter) extent on an "operational" basis. It will also provide verifiable estimates of individual live and senescent canopies in most situations. This implies that very large regions can be observed and processed without significant manual effort. Therefore, the approach could have major implications for monitoring arid and semiarid environments on a regular basis, an effort called for by the United Nations Environment Program (UNEP, 1992).

We thank Barbara Nolen for providing the Jornada vegetation map and the Sevilleta LTER personnel for providing their invaluable field data. We also thank the NASA EOS Validation PROVE campaign organizers and members for providing logistical support, data, and feedback for our study. This work was supported by NASA New Investigator Program grant NAG5-8709 and NASA Land-cover/Land-use Change grant NAG5-6134.

REFERENCES

Asner, G. P. (1998), Biophysical and biochemical sources of variability in canopy reflectance. *Remote Sens. Environ.* 64:234–253.

Asner, G. P., Braswell, B. H., Schimel, D. S., and Wessman, C. A. (1998a), Ecological research needs from multi-angle remote sensing data. *Remote Sens. Environ.* 63:155–165.

Asner, G. P., Wessman, C. A., Bateson, C. A., and Privette, J. L. (2000), Impact of tissue, canopy and landscape factors on reflectance variability of arid ecosystems. *Remote Sens. Environ*. 74:69–84.

Asner, G. P., Wessman, C. A., and Schimel, D. S. (1998b), Heterogeneity of savanna canopy structure and function from imaging spectrometry and inverse modeling. *Ecol. Applic*. 8:1022–1036.

Bateson, C. A., Asner, G. P., and Wessman, C. A. (2000), End-member bundles: A new approach to incorporating end-member variability in spectral mixture analysis. *IEEE Trans. Geosci. Remote Sens*. 38:1083–1094.

Ben-Dor, E., Irons, J. R., and Epema, G. F. (1999), Soil reflectance. In *Remote Sensing for the Earth Sciences* (A. N. Rencz, Ed.), John Wiley and Sons, New York, pp. 111–188.

Carlson, T. N., and Ripley, D. A. (1997), On the relation between NDVI, fractional vegetation cover, and leaf area index. *Remote Sens. Environ*. 62:241–255.

Caulfield, F., Britz, S. J., and Bunce, H. A. (1992), Shade spectral quality and the photosynthetic capacity of soybean leaves. *Photosynthetica* 26:555–568.

Clark, R. N. (1999), Spectroscopy of rocks and minerals, and principles of spectroscopy. In *Remote Sensing for the Earth Sciences* (A. N. Rencz, Ed.), John Wiley and Sons, New York, pp. 3–57.

Curran, P. J. (1989), Remote sensing of foliar chemistry. *Remote Sens. Environ.* 30:271–278.

Drake, N. A., Mackin, S., and Settle, J. J. (1999), Mapping vegetation, soils and geology in semiarid shrublands using spectral matching and mixture modeling of SWIR AVIRIS imagery. *Remote Sens. Environ.* 68:12–25.

Field, C. B., Randerson, J. T., and Malmstrom, C. T. (1995), Global net primary production: Combining ecology and remote sensing. *Remote Sens. Environ.* 51:74–88.

Gao, B.-C., Heidebrecht, K. B., and Goetz, A. F. H. (1993), Derivation of scaled surface reflectance from AVIRIS data. *Remote Sens. Environ.* 44:165–178.

Goetz, A. F. H., Vane, G., Solomon, J. E., and Rock, B. N. (1985), Imaging spectrometry for Earth remote sensing. *Science* 228:1147–1153.

Green, R. O., Eastwood, M. L., and Williams, O. (1998), Imaging spectroscopy and the Airborne Visible/Infrared Imaging Spectrometer (AVIRIS). *Remote Sens. Environ.* 65: 227–240.

Hall, F. G., Huemmrich, K. F., and Goward, S. N. (1990), Use of narrow-band spectra to estimate the fraction of absorbed photosynthetically active radiation. *Remote Sens. Environ*. 32:47–60.

Jacquemoud, S., Baret, F., and Hanocq, J. F. (1992), Modeling spectral and bidirectional soil reflectance. *Remote Sens. Envir.* 41:123–132.

Myneni, R. B., Los, S. O., and Tucker, C. J. (1996), Satellite-based identification of linked vegetation index and sea surface temperature anomaly areas from 1982–1990 for Africa, Australia and South America. *Geophys. Res. Lett.* 23:729–732.

Myneni, R. B., Nemani, R. R., and Running, S. W. (1997), Estimation of global leaf area index and absorbed PAR using radiative transfer models. *IEEE Trans. Geosci. Remote Sens*. 35:1380–1396.

Myneni, R. B., Ross, J., and Asrar, G. (1989), A review on the theory of photon transport in leaf canopies. *Agric. For. Meteor.* 45:1–153.

NMAES (1970), *Influence of Grazing Intensity on Improvement of Deteriorated Black Grama Range.* Bulletin 553. New Mexico Agricultural Experiment Station, Las Cruces, NM.

Pinty, B., Verstraete, M. M., and Gobron, N. (1998), The effect of soil anisotropy on the radiance field emerging from vegetation canopies. *Geophys. Res. Lett.* 25:797–800.

Ross, J. K. (1981), *The Radiation Regime and Architecture of Plant Stands.* Kluwer Academic, Boston, MA.

Running, S. W., Justice, C. O., Salomonson, V., Hall, D., Barker, J., Kaufmann, Y. J., Strahler, A. H., Huete, A. R., Muller, J. P., Vanderbilt, V., Wan, Z. M., Teillet, P., and Carnegie, D. (1994), Terrestrial remote sensing science and algorithms planned for EOS/MODIS. *Int. J. Remote Sens.* 15:3587–3620.

Schlesinger, W. H., and Pilmanis, A. M. (1998), Plant-soil interactions in deserts. *Biogeochemistry* 42:169–87.

Schlesinger, W. H., Raikes, J. A., and Cross, A. F. (1996), On the spatial pattern of soil nutrients in desert ecosystems. *Ecology* 77:364–376.

Schlesinger, W. H., Reynolds, J. F., Cunningham, G. L., Huenneke, L. F., Jarrell, W. M., Virginia, R. A., and Whitford, W. G. (1990), Biological feedbacks in global desertification. *Science* 247:1043–1048.

Smith, M. O., Adams, J. B., and Sabol, D. E. (1994), Spectral mixture analysis-new strategies for the analysis of multispectral data. In *Imaging Spectrometry—A Tool for Environmental Observations* (J. Hill and J. Megier, Eds.), Kluwer Academic, Dordrecht, The Netherlands, pp. 125–144.

Tucker, C. J., Dregne, H. E., and Newcomb, W. W. (1991), Expansion and contraction of the Sahara Desert from 1980 to 1990. *Science* 253:299–301.

UNEP (1992), *Status of Desertification and Implementation of the United Nations Plan of Action to Combat Desertification.* United Nations Environment Programme, Nairobi, Kenya.

USDA (1934), *The Influence of Precipitation and Grazing on Black Grama Range.* Technical Bulletin 409, U.S. Department of Agriculture.

Ustin, S. L., Smith, M. O., Jacquemoud, S. (1999), Geobotany: Vegetation mapping for earth sciences. In *Remote Sensing for the Earth Sciences* (A. N. Rencz, Ed.), John Wiley and Sons, New York.

van Leeuwen, W. J. D., and Huete, A. R. (1996), Effects of standing litter on the biophysical interpretation of plant canopies with spectral indices. *Remote Sens. Environ.* 55: 123–134.

van Leeuwen, W. J. D., Huete, A. R., Walthall, C. L., Prince, S. D., Begue, A., and Roujeau, J.-L. (1997), Deconvolution of remotely sensed spectral mixtures for retrieval of LAI, FPAR, and soil brightness. *Journal of Hydrology* 188/ 189:697–724.

Vermote, E. F., Tanre, D., Deuze, J. L., Herman, M., and Morcrette, J. J. (1997), Second simulation of the satellite signal in the solar spectrum, 6S: An overview. *IEEE Trans. Geosci. Remote Sens*. 35:675–699.

Wessman, C. A., and Asner, G. P. (1998), Ecosystems and the problems of large-scale measurements. In *Successes, Limitations, and Frontiers in Ecosystem Ecology* (P. Groffman and M. Pace, Eds.), Springer-Verlag, Berlin, pp. 346–371.

Wessman, C. A., Bateson, C. A., and Benning, T. L. (1997), Detecting fire and grazing patterns in tallgrass prairie using spectral mixture analysis. *Ecol. Appl.* 7:493–511.

White, M. A., Asner, G. P., Nemani, R. R., Privette, J. L., and Running, S. W. (2000), Monitoring fractional cover and leaf area index in arid ecosystems: Digital camera, radiation transmittance, and laser altimetry results. *Remote Sens. Environ.* 74:45–57.

Wooley, J. T. (1971), Reflectance and transmittance of light by leaves. *Plant Physiol.* 47:656–662.